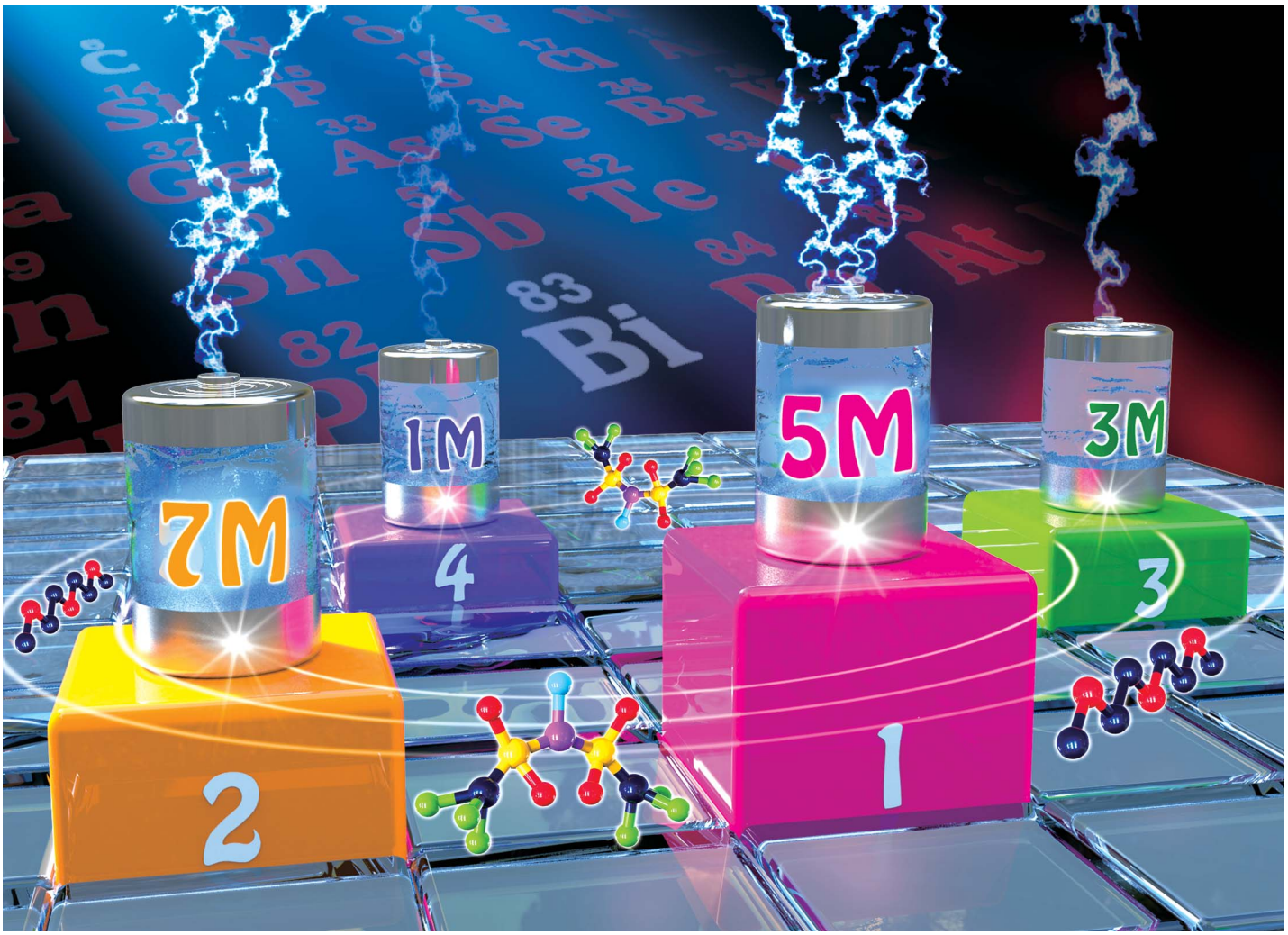

Showcasing research from Professor Chuan-Fu Sun's laboratory, Fujian Institute of Research on the Structure of Matter, Chinese Academy of Sciences, Fuzhou, China.

Concentrated electrolytes stabilize bismuth–potassium batteries

A 5 molar concentrated electrolyte effectively stabilizes bismuth-potassium batteries due to its elevated resistance to electrochemical reduction. This protection allows the simultaneous achievements of high specific capacity, robust electrochemical cyclability, and improved rate capability, which are not possible with the typical 1 molar or excessively concentrated 7 molar electrolytes.

As featured in:

See Chuan-Fu Sun *et al.*, *Chem. Sci.*, 2018, **9**, 6193.

ROYAL SOCIETY OF CHEMISTRY

rsc.li/chemical-science

Registered charity number: 207890

Chemical Science

EDGE ARTICLE

View Article Online
View Journal | View Issue

Cite this: *Chem. Sci.*, 2018, **9**, 6193

Concentrated electrolytes stabilize bismuth–potassium batteries†

Ruding Zhang,[a] Jingze Bao,[a] YuHuang Wang[b] and Chuan-Fu Sun *[a]

Storing as many as three K-ions per atom, bismuth is a promising anode material for rechargeable potassium-ion batteries that may replace lithium-ion batteries for large-scale electrical energy storage. However, Bi suffers from poor electrochemical cyclability in conventional electrolytes. Here, we demonstrate that a 5 molar (M) ether-based electrolyte, *versus* the typical 1 M electrolyte, can effectively passivate the bismuth surface due to elevated reduction resistance. This protection allows a bismuth–carbon anode to simultaneously achieve high specific capacity, electrochemical cyclability and Coulombic efficiency, as well as small potential hysteresis and improved rate capability. We show that at a high electrolyte concentration, the bismuth anode demonstrates excellent cyclability over 600 cycles with 85% capacity retention and an average Coulombic efficiency of 99.35% at 200 mA g^{-1}. This "concentrated electrolyte" approach provides unexpected new insights to guide the development of long-cycle-life and high-safety potassium-ion batteries.

Received 23rd April 2018
Accepted 16th June 2018

DOI: 10.1039/c8sc01848k

rsc.li/chemical-science

Introduction

Rechargeable potassium-ion batteries (PIBs) are a promising alternative to lithium-ion batteries (LIBs) for large-scale electrical energy storage because of the abundance of potassium resources, low cost, and environmental benignity.[1–7] However, their development has been hindered by the lack of appropriate electrode materials that could reversibly store K-ions.[2,6–9] For the cathode, layered transition metal oxides,[10–12] transition metal sulfides/phosphates,[13–15] and Prussian blue and its analogs have been intensively investigated, and they show promising prospects.[4,16–19] In particular, due to a framework structure, Prussian blue and its analogs could effectively accommodate the structural changes induced by K-ion insertion/extraction and exhibit relatively high capacity, cell voltage, and cyclability.[4,16–19] For the anode, several materials have been intensively studied, including carbonaceous materials (*i.e.*, graphite, graphene, and hard/soft carbon),[3,20–24] organic anode materials,[25,26] alloy-type metals (*i.e.*, Sb, Sn, and Sn_4P_3),[27–30] metal oxides/sulfides,[31–35] and metal phosphates (*i.e.*, $KTi_2(PO_4)_3$).[36] However, none of these anode materials are yet to achieve electrochemical performances that match that of Prussian blue and its analogs on the cathode side.

Very recently, Guo *et al.* and Chen *et al.* showed that each bismuth (Bi) can store three K^+ maximum *via* forming a K_3Bi alloy.[37,38] This alloy reaction, in theory, gives specific and volumetric capacities of 385 mA h g^{-1} and 1147 mA hcm^{-3}, respectively, both of which are significantly higher than those of graphite, Sn and $KTi_2(PO_4)_3$ (Fig. 1). Equally important is that this new battery chemistry operates at an average potential of ~0.6 V *versus* K/K^+, making it intrinsically free from potassium plating which may cause catastrophic battery failure. These merits together with low cost and nontoxic features make Bi a promising candidate anode material for PIBs.[37–40] However,

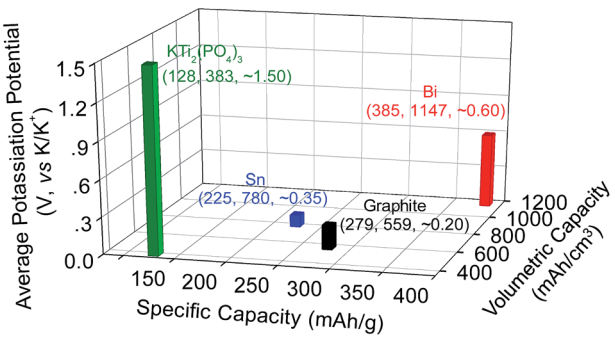

Fig. 1 Potassium-ion storage potential of Bi compared to that of graphite, Sn, and $KTi_2(PO_4)_3$. The (*x*, *y*, *z*) coordinates represent the theoretical specific capacity, theoretical volumetric capacity, and average operation potential, respectively. All the specific capacities are calculated based on the mass of the active material, while the volumetric capacities are calculated based on the volume and density of the final potassiated phase (K_3Bi, KC_8, and KSn) except $KTi_2(PO_4)_3$ whose value is estimated based on the original phase as its potassiated structure remains unknown.

[a]*CAS Key Laboratory of Design and Assembly of Functional Nanostructures, Fujian Provincial Key Laboratory of Nanomaterials, Fujian Institute of Research on the Structure of Matter, Chinese Academy of Sciences, Fuzhou, Fujian, 350002, P. R. China. E-mail: cfsun@fjirsm.ac.cn*

[b]*Department of Chemistry and Biochemistry, University of Maryland, College Park, Maryland 20742, USA*

† Electronic supplementary information (ESI) available. See DOI: 10.1039/c8sc01848k

similar to other high capacity alloy anodes, the phase transformation from Bi to K_3Bi presents a volume expansion of ~400%. Such a large volume change inevitably decreases the stabilities of both the structure and solid electrolyte interphase (SEI) formed on the Bi surface, inducing rapid capacity decay upon electrochemical cycling in conventional electrolytes. This problem is similar to those observed in LIBs, but it is even more challenging due to the large ionic radius of K^+ (1.38 Å), which is 81.6% larger than that of Li^+.[7]

Here, we show that a bismuth–carbon anode operating in a 5 M concentrated electrolyte of potassium bis(trifluoromethylsulfonyl)imide (KTFSI) in diethylene glycol dimethyl ether (DEGDME) simultaneously achieves high specific capacity, cyclability, and Coulombic efficiency, small potential hysteresis and improved rate capability well beyond those of the typical 1 M electrolyte. We also found that an even higher electrolyte concentration (7 M) results in similar cyclability, potential hysteresis and Coulombic efficiency for the Bi@C nanocomposite anode, but its K-ion storage capacity and rate capability are largely sacrificed. These results uncover an unexpected critical role of electrolyte chemistry in Bi–K batteries.

Results and discussion

The phase purity and crystallinity of the as-synthesized bismuth–carbon (Bi@C) nanocomposites were confirmed by X-ray powder diffraction (XRD) (Fig. 2a). All the diffraction peaks shown in the XRD pattern can be indexed to the rhombohedral phase with a space group of $R\bar{3}m$. The corresponding crystal structure of Bi is shown in the inset of Fig. 2a. Scanning electron microscopy (SEM) and high-resolution transmission electron microscopy (HRTEM) images show that the Bi nanoparticles have an average diameter of ~30 nm while the carbon coating is roughly 15 nm thick (Fig. 2b–d, S1, ESI†). The content of Bi in these Bi@C materials is 85.6 wt%, as revealed by thermogravimetric analysis (Fig. S2, ESI†). These Bi@C materials were mixed with Super-P carbon black and a carboxymethyl cellulose binder to fabricate the electrodes based on a slurry-coating process. The mass loading of Bi in the electrodes is ~1.3 mg cm^{-2}. The Bi@C anodes together with carbon black and the binder were directly peeled from Al current collectors for Brunauer–Emmett–Teller (BET) measurements, which give a specific surface area of 24.7 $m^2\ g^{-1}$ for the bulk anode (Fig. S3, ESI†).

To evaluate the electrolyte-concentration effect on electrochemical performances, the Bi@C anodes were coupled with K-foil and the KTFSI–DEGDME electrolytes (1 M, 5 M and 7 M) to fabricate PIB half-cells which subsequently underwent galvanostatic cycling. As shown in Fig. 3a and b, at a low rate of 10 mA g^{-1} (~0.025C), the Bi@C anode delivers an initial reversible depotassiation capacity of 227 mA h g^{-1} with an initial Coulombic efficiency (CE) of 46.3% under the 5 M electrolyte. Note that all the capacities herein were calculated based on the mass of Bi@C. The low initial CE is commonly observed in alloy-type anodes and could be attributed to the formation of the SEI.[29,37] After five-cycle activation, a reversible depotassiation capacity of 250 mA h g^{-1} was achieved in the 6th cycle. This high specific capacity is comparable to that of graphitic anodes and a bit higher than those of Sn, MoS_2, and Ti-based oxides/phosphates.[3,20,31–33,36] In contrast, when the 1 M electrolyte was applied, the Bi@C anode shows a lower initial reversible depotassiation capacity of 171 mA h g^{-1} and a lower initial CE of

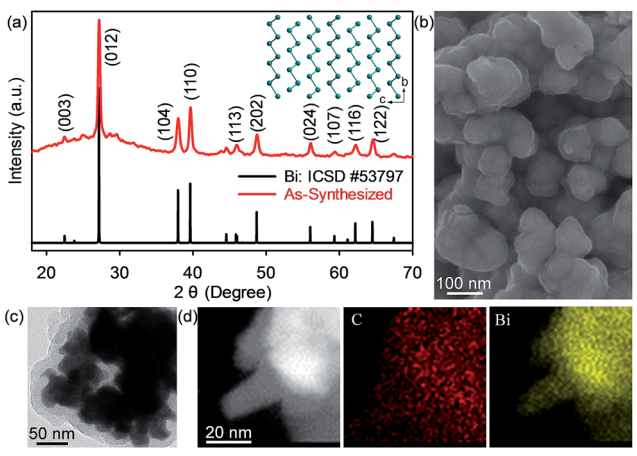

Fig. 2 XRD and electron microscopy characterization of the Bi@C nanocomposite: (a) XRD confirming the purity and crystallinity of Bi@C. The inset shows the crystal structure of Bi. (b) SEM image, (c) TEM image, and (d) dark-field TEM EDS mapping of the Bi@C nanocomposite.

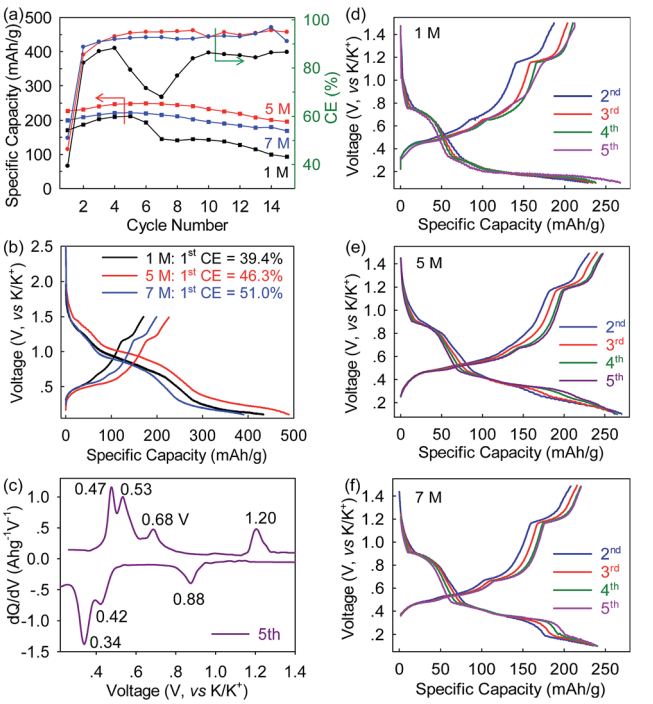

Fig. 3 The electrochemical discrepancy of the Bi@C anode at 10 mA g^{-1} in different electrolyte concentrations: (a) Depotassiation capacity and Coulombic efficiency (CE). (b) First-cycle voltage profiles. (c) dQ/dV curve in the 5th cycle in the 5 M KTFSI–DEGDME electrolyte. (d–f) Galvanostatic voltage profiles in the 1 M (d), 5 M (e), and 7 M (f) KTFSI–DEGDME electrolytes.

39.4% while with even more concentrated 7 M electrolyte, the highest initial CE of 51.0% and a moderately high initial depotassiation capacity of 199 mA h g^{-1} were achieved. The capacity retention after 15 cycles is similar for concentrated electrolytes (78% for 5 M and 76% for 7 M), nearly twice that with the 1 M electrolyte (44%). These discrepancies evidently reveal that electrochemical performances strongly depend on the electrolyte concentration. When the appropriate electrolyte concentration is used, the K-ion storage capacity and cyclability of the Bi@C anode can be significantly elevated. In addition, all the KTFSI–DEGDME electrolytes outperform the electrolyte of KPF_6 in an ester-based solvent (the capacity completely decays within 5 cycles, as shown in Fig. S4, ESI†), consistent with previous reports.[25,37,38] With the optimized 5 M electrolyte, three cathodic peaks (at around 0.88, 0.42, and 0.34 V) and the corresponding anodic ones (at around 1.20, 0.68, 0.53, and 0.47 V) observed in the dQ/dV curve indicate a small potential hysteresis (the gap between the cathodic and the corresponding anodic peak) of 0.16–0.32 V (Fig. 3c). This value is similar to that in the 7 M (0.16–0.30 V) electrolyte and smaller than that in the 1 M electrolyte (0.33–0.47 V) (Fig. 3, S5, ESI†), which indicates that concentrated electrolytes can depress the potential hysteresis in Bi@C anodes and thus, in theory, allow the Bi–K battery chemistry to achieve higher energy efficiency. The presence of multiple cathodic/anodic peaks also indicates that this Bi–K battery chemistry may undergo a multi-step reaction which will be discussed in detail later in this paper. In addition, the Bi@C anode exhibits an average potassiation potential of ~0.60 V, which makes it intrinsically free from potassium plating, and thus improves safety over graphite and Sn.[3,28]

Apart from the positive impact on safety, the electrolyte concentration also evidently improves the long-term cyclability of the Bi@C anodes. At a rate of 50 mA g^{-1} (~0.14C), the Bi@C anode in the 5 M electrolyte delivers a maximum reversible capacity of 220 mA h g^{-1} after a few cycles of activation, and 88% of the capacity remains in the 20th cycle (Fig. 4a). In contrast, the corresponding capacity retention of the Bi@C anode in the 1 M and 3 M electrolytes is as low as 25% and 69%, respectively, while in the 7 M electrolyte, an even higher capacity retention of 92% can be achieved, but the reversible capacity was significantly compromised (90 mA h g^{-1}). The same trend was observed at a rate of 100 mA h g^{-1}. As shown in Fig. 4b, the reversible capacities in the 35th cycle are 10, 67, 151, and 36 mA h g^{-1} for the 1 M, 3 M, 5 M, and 7 M electrolytes, respectively, with a capacity retention of 10%, 49%, 85%, and 90%. These results again demonstrate the vital role of appropriate electrolyte concentration in the Bi–K battery chemistry. In the 5 M electrolyte, the Bi@C anode achieves excellent cyclability over 600 cycles with 85% capacity retention and an average Coulombic efficiency (from the 2nd to the 600th cycle) of 99.35% at 200 mA g^{-1} (Fig. 4c).

At the 5 M electrolyte concentration, the rate capability of the Bi@C anode is also optimal. Excess electrolyte concentration can adversely affect the rate capability of Bi@C anodes. As shown in Fig. 4d–f and S6,† the depotassiation capacities of the Bi@C anodes vary slightly in the 1 M, 3 M, 5 M, and 7 M electrolytes at a low rate of 10 mA g^{-1}. However, at a higher rate of

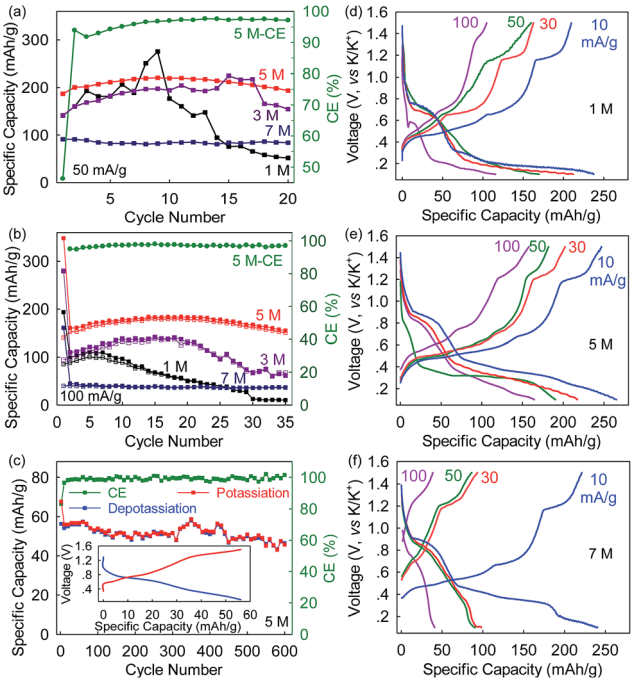

Fig. 4 Electrolyte concentration effects on electrochemical cyclability and rate capability of the Bi@C anode: (a) Depotassiation capacity and Coulombic efficiency at 50 mA g^{-1}. (b) Cyclability at 100 mA g^{-1}. Solid and empty squares represent the potassiation and depotassiation capacities, respectively. (c) Long-term cyclability at 200 mA g^{-1} in the 5 M KTFSI–DEGDME electrolyte. For clarity, the first cycle is not shown. (d–f) Rate capability in the 1 M (a), 5 M (b), and 7 M (c) KTFSI–DEGDME electrolytes.

30 mA g^{-1}, the Bi@C anode in the 5 M electrolyte exhibits a depotassiation capacity of 202 mA h g^{-1} which is higher than those in the 1 M and 3 M electrolytes (163 and 153 mA h g^{-1}, respectively) and more than twice that in the 7 M electrolyte (93 mA h g^{-1}). This capacity discrepancy becomes more prominent at an even higher rate. At 100 mA g^{-1}, the Bi@C anode in the 5 M electrolyte can still deliver a relatively high depotassiation capacity of 158 mA h g^{-1}, which cannot be achieved in the 1 M, 3 M or 7 M electrolytes. In particular, this capacity is four times as high as that in the 7 M electrolyte (39 mA h g^{-1}).

This strong concentration dependence mainly, if not solely, arises from the electrolytes themselves as other components including the anode remain identical. Previous reports have suggested that DME molecules in a concentrated KFSI-DME electrolyte tend to donate the lone-pair electrons of oxygen to solvated K-ions.[41] This behavior lowers the energy level of the highest occupied molecular orbital (HOMO) of DME and thus increases its redox resistance which is more than that of free DME in the low-concentration electrolyte.[41] We speculated that, similar to DME, the long-chain DEGDME molecules in the concentrated electrolytes possess higher resistance to electrochemical reduction and consequently form less solid electrolyte interphase on the Bi@C surface. This speculation is experimentally confirmed by linear sweep voltammetry (LSV) and *ex situ* SEM studies. As shown in Fig. 5a and b, the 1 M electrolyte shows a large reduction current of 0.022 mA at 0 V *versus* K/K^+.

In sharp contrast, the reduction current in the concentrated 3 M, 5 M, and 7 M electrolytes significantly reduces to 0.010, 0.009 and 0.008 mA, respectively, which are only 45.5%, 41% and 36% of that in the 1 M electrolyte. These results reveal that the reduction resistance of the KTFSI–DEGDME electrolyte is proportional to its concentration. The SEI formation behavior shown in Fig. 5c–i further confirms this concentration dependency. After one potassiation/depotassiation cycle, a thick SEI layer was observed on the surface of the Bi@C anode in the 1 M electrolyte, making the anode surface barely visible. Conversely, much less SEI formation was observed in the concentrated 5 M and 7 M electrolytes, and the anode morphology is distinctly recognizable (Fig. 5f–i). In other words, the significantly improved reduction resistance of the 5 M electrolyte depresses the irreversible electrochemical reaction and contributes to less formation of the SEI, higher reversible capacity, cyclability and Coulombic efficiency beyond those of the typical 1 M electrolyte. Furthermore, a thinner SEI layer enables faster K-ion diffusion across it and thus smaller potential hysteresis and improved rate capability.

To gain kinetic insights into the Bi@C anode in the 5 M electrolyte, electrochemical impedance spectroscopy (EIS) and galvanostatic intermittent titration technique (GITT) experiments were conducted, and the results are presented in Fig. 6 and S6.† The intercept of the Nyquist plots on the horizontal axis describes the electrolyte resistance (R_e) which is 11.77 Ω after three-cycle activation (Fig. 6c, S7, ESI†). The high-frequency depressed semicircle presents the total resistances of contact (R_f) and charge transfer (R_{ct}), while the low-frequency slope line accounts for Warburg ion-diffusion resistance (Z_w).[42] After three-cycle activation, the R_f was observed to be 10.3 Ω. This R_f is related to the ion-diffusion resistance across the SEI layer formed on the Bi@C surface, and its small value is a strong indication of well-developed electrolyte/electrode interfacial

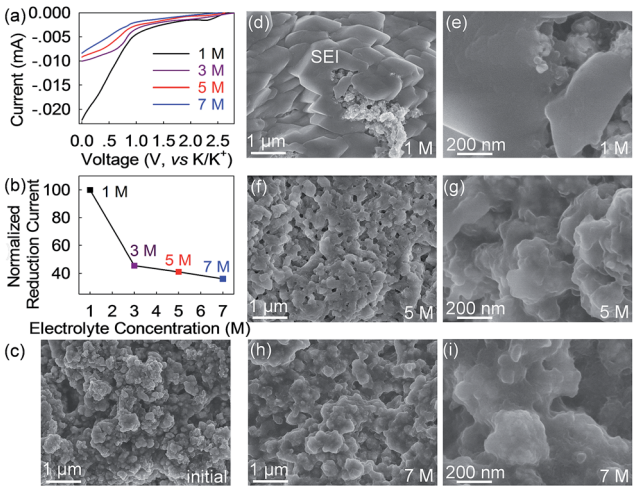

Fig. 5 Concentration-dependent reduction resistance of electrolytes: (a) linear sweep voltammetry (LSV) curves. (b) Normalized reduction current *versus* electrolyte concentration. (c–i) SEM images of the Bi@C anode. The initial anode (c) and anodes after one potassiation/depotassiation cycle in the 1 M (d and e), 5 M (f and g), and 7 M (h and i) KTFSI–DEGDME electrolytes.

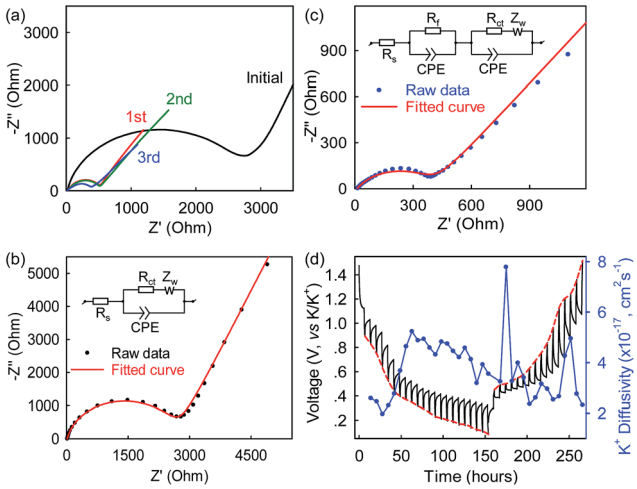

Fig. 6 Reaction kinetics study of the Bi@C nanocomposite anode in the 5 M KTFSI–DEGDME electrolyte: (a) EIS of the initial and cycled Bi@C anodes. (b and c) EIS fitting data of the initial (b) and three times cycled Bi@C anodes (c), where R_s, R_f, R_{ct}, CPE, and Z_w represent the electrolyte resistance, contact resistance, charge-transfer resistance, constant-phase element, and Warburg ion-diffusion resistance, respectively. The insets of (b) and (c) show the corresponding equivalent circuits used for the data fitting. (d) GITT data collected during the 2nd cycle.

contact and relatively fast K^+ permeation through the SEI film. The R_{ct} was estimated to be 408.9 Ω which is nearly 10 times lower than that observed in the graphite anode (4358 Ω),[23] suggesting relatively fast charge transfer in the Bi@C anode. Note that the electrolyte resistance (R_e) in the 7 M electrolyte is ~22 Ω which is about twice that in the 5 M electrolyte (Fig. S8, ESI†). This large resistance results in sluggish K-ion transport in the over-concentrated 7 M electrolyte and could account for the lower capacity and rate capability, compared with the 5 M electrolyte. In addition, as shown in Fig. 6d, the chemical diffusion coefficients of K-ions ($D_{K\text{-ion}}$) in the Bi@C electrode under the 5 M electrolyte were also estimated based on the GITT measurements and the surface area of the bulk anode. The $D_{K\text{-ion}}$ values vary to some extent during cycling and are on the order of $\sim 10^{-17}$ cm^2 s^{-1}. This small $D_{K\text{-ion}}$ can be attributed to the large size of K-ions (1.38 Å in ionic radius, 81.6% larger than that of Li^+). Note that the ion diffusion coefficients are sometimes calculated based on the geometric area of electrodes and are usually several orders of magnitude higher. The $D_{K\text{-ion}}$ values here are calculated to be $\sim 10^{-12}$ cm^2 s^{-1} based on the geometric area of the anode.

The electrochemical reaction mechanism of the Bi–K battery chemistry was also investigated through *ex situ* XRD tests (Fig. 7). Upon potassiation at 0.8 V and 0.5 V, the XRD signals of KBi and unreacted Bi are detected. As the potassiation is extended to 0.1 V, a new signal of K_3Bi appears. In the reversible process, the K_3Bi phase coexists with KBi upon depotassiation at 0.5 V and disappears at 0.8 V. Upon further depotassiation at 1.5 V, nearly all K^+ have been removed, and Bi dominates the detectable phase. Based on the experimental observations in the *ex situ* XRD study, the Bi–K battery chemistry may undergo

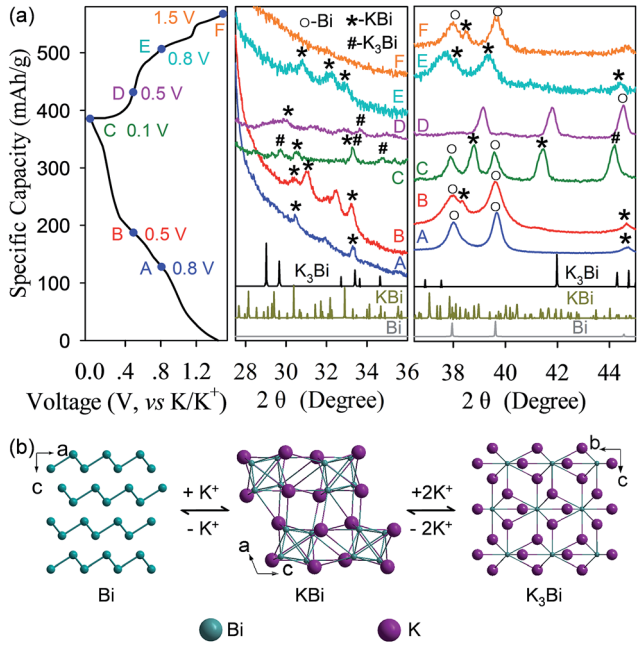

Fig. 7 Mechanistic studies of the Bi@C anode in the 5 M KTFSI–DEGDME electrolyte: (a) *Ex situ* XRD recorded during the first cycle. The results reveal evidence of a multi-step reaction involving the phase transformation of Bi metal to the KBi alloy and ultimately to the K_3Bi alloy. (b) Schematics illustrating the phase transformation of Bi upon potassiation/depotassiation.

two-phase reactions which involve the phase transformation of Bi metal to the KBi alloy and eventually the K_3Bi alloy upon potassiation and a reversible process upon depotassiation (Fig. 7b). It is interesting to note that this reaction mechanism is distinctly different from those reported previously.[37,38] Particularly, Guo *et al.* found that the Bi–K battery chemistry undergoes two-phase reactions as well, but the reactions experience the transformation of Bi to K_5Bi_4 and ultimately K_3Bi,[37] while in another work, Chen *et al.* observed a three-phase transformation from Bi to KBi_2, K_3Bi_2, and K_3Bi.[38] The discrepancy in reaction mechanisms indicates that the Bi–K battery chemistry may undergo multi-phase (more than three-phase) reactions. Further studies are needed to resolve this discrepancy. Nevertheless, in all of these cases, the observed ultimate potassiation phase is always K_3Bi, corresponding to a maximum K-ion storage capacity as high as 385 mA h g^{-1}.

Conclusions

In summary, we propose a "concentrated electrolyte" approach to achieve significantly improved electrochemical storage performance for bismuth–potassium batteries. Our results show that a 5 M (*versus* the typical 1 M) ether-based electrolyte can effectively passivate the bismuth–carbon surface by increasing its reduction resistance. This protection enables the realization of a bismuth–potassium battery with a significantly higher reversible capacity (250 mA h g^{-1} at 10 mA g^{-1}), electrochemical cyclability and Coulombic efficiency (up to 600 cycles with 85% capacity retention and an average CE of 99.35% at 200 mA g^{-1}), as well as depressed potential hysteresis and improved rate capability. This approach paves the way for the incorporation of high capacity anode materials and innovative electrolytes into rechargeable potassium-ion batteries.

Conflicts of interest

The authors declare no competing financial interest.

Acknowledgements

This work is financially supported by the National Natural Science Foundation of China (Grant No. 21771180 and 51702318) and Natural Science Foundation of Fujian Province (Grant No. 2018J01031), and in part by Nanostructures for Electrical Energy Storage (NEES), an Energy Frontier Research Center funded by the U.S. Department of Energy, Office of Science, Office of Basic Energy Sciences under Award Number DESC0001160.

Notes and references

1 A. Eftekhari, *J. Power Sources*, 2004, **126**, 221–228.
2 A. Eftekhari, Z. Jian and X. Ji, *ACS Appl. Mater. Interfaces*, 2017, **9**, 4404–4419.
3 Z. Jian, W. Luo and X. Ji, *J. Am. Chem. Soc.*, 2015, **137**, 11566–11569.
4 L. Xue, Y. Li, H. Gao, W. Zhou, X. Lu, W. Kaveevivitchai, A. Manthiram and J. B. Goodenough, *J. Am. Chem. Soc.*, 2017, **139**, 2164–2167.
5 Q. Zhao, J. Wang, Y. Lu, Y. Li, G. Liang and J. Chen, *Angew. Chem., Int. Ed.*, 2016, **55**, 12528–12532.
6 H. Kim, J. C. Kim, M. Bianchini and D. H. Seo, *Adv. Energy Mater.*, 2017, 1702384.
7 X. Wu, D. P. Leonard and X. Ji, *Chem. Mater.*, 2017, **29**, 5031–5042.
8 J. C. Pramudita, D. Sehrawat, D. Goonetilleke and N. Sharma, *Adv. Energy Mater.*, 2017, 1602911.
9 X. Zou, P. Xiong, J. Zhao, J. Hu, Z. Liu and Y. Xu, *Phys. Chem. Chem. Phys.*, 2017, **19**, 26495–26506.
10 C. Vaalma, G. A. Giffin, D. Buchholz and S. Passerini, *J. Electrochem. Soc.*, 2016, **163**, A1295–A1299.
11 X. Wang, X. Xu, C. Niu, J. Meng, M. Huang, X. Liu, Z. Liu and L. Mai, *Nano Lett.*, 2017, **17**, 544–550.
12 H. Kim, J. C. Kim, S. H. Bo, T. Shi, D. H. Kwon and G. Ceder, *Adv. Energy Mater.*, 2017, **7**, 1700098.
13 B. Tian, W. Tang, K. Leng, Z. Chen, S. J. R. Tan, C. Peng, G. H. Ning, W. Fu, C. Su, G. W. Zheng, *et al.*, *ACS Energy Lett.*, 2017, **2**, 1835–1840.
14 K. Chihara, A. Katogi, K. Kubota and S. Komaba, *Chem. Commun.*, 2017, **53**, 5208–5211.
15 V. Mathew, S. Kim, J. Kang, J. Gim, J. Song, J. P. Baboo, W. Park, D. Ahn, J. Han, L. Gu, *et al.*, *NPG Asia Mater.*, 2014, **6**, e138.
16 Y. H. Zhu, Y. B. Yin, X. Yang, T. Sun, S. Wang, Y. S. Jiang, J. M. Yan and X. B. Zhang, *Angew. Chem., Int. Ed.*, 2017, **56**, 7881–7885.

17 G. He and L. F. Nazar, *ACS Energy Lett.*, 2017, **2**, 1122–1127.
18 Z. Shadike, D. R. Shi, T. Wang, M. H. Cao, S. F. Yang, J. Chen and Z. W. Fu, *J. Mater. Chem. A*, 2017, **5**, 6393–6398.
19 D. Su, A. McDonagh, S. Z. Qiao and G. Wang, *Adv. Mater.*, 2017, **29**, 1604007.
20 W. Luo, J. Wan, B. Ozdemir, W. Bao, Y. Chen, J. Dai, H. Lin, Y. Xu, F. Gu, V. Barone, *et al.*, *Nano Lett.*, 2015, **15**, 7671–7677.
21 Z. Jian, Z. Xing, C. Bommier, Z. Li and X. Ji, *Adv. Energy Mater.*, 2016, **6**, 1501874.
22 Z. Jian, S. Hwang, Z. Li, A. S. Hernandez, X. Wang, Z. Xing, D. Su and X. Ji, *Adv. Funct. Mater.*, 2017, **27**, 1700324.
23 J. Zhao, X. Zou, Y. Zhu, Y. Xu and C. Wang, *Adv. Funct. Mater.*, 2016, **26**, 8103–8110.
24 J. Yang, Z. Ju, Y. Jiang, Z. Xing, B. Xi, J. Feng and S. Xiong, *Adv. Mater.*, 2018, **30**, 1700104.
25 K. Lei, F. Li, C. Mu, J. Wang, Q. Zhao and C. J. Chen, *Energy Environ. Sci.*, 2017, **10**, 552–557.
26 Q. Deng, J. Pei, C. Fan, J. Ma, B. Cao, C. Li, Y. Jin, L. Wang and J. Li, *Nano Energy*, 2017, **33**, 350–355.
27 W. D. McCulloch, X. Ren, M. Yu, Z. Huang and Y. Wu, *ACS Appl. Mater. Interfaces*, 2015, **7**, 26158–26166.
28 I. Sultana, T. Ramireddy, M. M. Rahman, Y. Chen and A. M. Glushenkov, *Chem. Commun.*, 2016, **52**, 9279–9282.
29 W. Zhang, J. Mao, S. Li, Z. Chen and Z. Guo, *J. Am. Chem. Soc.*, 2017, **139**, 3316–3319.
30 Q. Wang, X. Zhao, C. Ni, H. Tian, J. Li, Z. Zhang, S. X. Mao, J. Wang and Y. Xu, *J. Phys. Chem. C*, 2017, **121**, 12652–12657.
31 X. Ren, Q. Zhao, W. D. McCulloch and Y. Wu, *Nano Res.*, 2017, **10**, 1313–1321.
32 J. Han, M. Xu, Y. Niu, G. N. Li, M. Wang, Y. Zhang, M. Jia and C. M. Li, *Chem. Commun.*, 2016, **52**, 11274–11276.
33 B. Kishore, V. G and N. Munichandraiah, *J. Electrochem. Soc.*, 2016, **163**, A2551–A2554.
34 H. Gao, T. Zhou, Y. Zheng, Q. Zhang, Y. Liu, J. Chen, H. Liu and Z. Guo, *Adv. Funct. Mater.*, 2017, **27**, 1702634.
35 J. Zhou, L. Wang, M. Yang, J. Wu, F. Chen, W. Huang, N. Han, H. Ye, F. Zhao, Y. Li, *et al.*, *Adv. Mater.*, 2017, **29**, 1702061.
36 J. Han, Y. Niu, S. J. Bao, Y. N. Yu, S. Y. Lu and M. Xu, *Chem. Commun.*, 2016, **52**, 11661–11664.
37 Q. Zhang, J. Mao, W. K. Pang, T. Zheng, V. Sencadas, Y. Chen, Y. Liu and Z. Guo, *Adv. Energy Mater.*, 2018, 1703288.
38 K. Lei, C. Wang, L. Liu, Y. Luo, C. Mu, F. Li and J. Chen, *Angew. Chem., Int. Ed.*, 2018, **57**, 4687.
39 C. F. Sun, J. Hu, P. Wang, X. Y. Cheng, S. B. Lee and Y. Wang, *Nano Lett.*, 2016, **16**, 5875–5882.
40 J. Huang, X. Lin, H. Tan and B. Zhang, *Adv. Energy Mater.*, 2018, 1703496.
41 N. Xiao, W. D. McCulloch and Y. Wu, *J. Am. Chem. Soc.*, 2017, **139**, 9475–9478.
42 C. F. Sun, H. Zhu, E. B. Baker III, M. Okada, J. Wan, A. Ghemes, Y. Inoue, L. Hu and Y. Wang, *Nano Energy*, 2013, **2**, 987–994.